Available online at www.sciencedirect.com
SCIENCE DIRECT
Polymer 47 (2006) 2772–2790
polymer
www.elsevier.com/locate/polymer

Compatibilisation of PPE/SAN blends by triblock terpolymers: Correlation between block terpolymer composition, morphology and properties

Holger Ruckdäschel [a], Jan K.W. Sandler [a], Volker Altstädt [a,*], Cornelia Rettig [b], Holger Schmalz [b], Volker Abetz [b,1], Axel H.E. Müller [b,**]

[a] *Polymer Engineering, University of Bayreuth, D-95440 Bayreuth, Germany*
[b] *Macromolecular Chemistry II, University of Bayreuth, D-95440 Bayreuth, Germany*

Received 16 December 2005; received in revised form 13 February 2006; accepted 21 February 2006
Available online 14 March 2006

Abstract

Immiscible blends of poly(2,6-dimethyl-1,4-phenylene ether) (PPE) and poly(styrene-*co*-acrylonitrile) (SAN) with a weight composition of 60/40 were compatibilised by polystyrene-*block*-polybutadiene-*block*-poly(methyl methacrylate) triblock terpolymers (SBM) using a two-stage melt-processing approach. In order to investigate the influence of the SBM composition on the compatibilisation efficiency, the block lengths of the triblock terpolymers were systematically varied. The resulting morphological features of the blend systems as function of SBM composition and processing parameters are correlated with the resulting thermal and thermo-mechanical properties. In the ideal case, SBM should be located at the interface as PS is miscible with PPE while PMMA is miscible with SAN. The elastomeric middle block as an immiscible component should remain at the interface. This particular morphological arrangement is known as the 'raspberry morphology'. A detailed TEM analysis of the blend morphologies following initial extrusion-compounding revealed a high compatibilisation efficiency of the SBM types with equal lengths of the end blocks and, furthermore, the desired raspberry morphology was achieved. In contrast, high PS contents in comparison to the other blocks led to a pronounced micelle formation in the PPE phase. Further evaluation of the blend structures following injection-moulding indicated that the morphologies remain relatively stable during this second melt-processing step. A detailed thermal analysis of all blend systems supports the interpretation of the observed morphological features. The fundamental correlation between SBM composition and blend morphology established in this study opens the door for the controlled development of interfacial properties of such compatibilised PPE/SAN blends during melt-processing.

Keywords: Polymer blend; Compatibilisation; Triblock terpolymer

1. Introduction

Blending of polymers provides an efficient route to develop new materials with tailored properties [1,2]. Due to the fact that an already existing range of base polymers is used, a large variety of new high-capacity polymers is readily and economically available. The highest market value and the strongest growth rate are predicted for blends based on both polycarbonate (PC) and poly(2,6-dimethyl-1,4-phenylene ether) (PPE). It should be noted that PPE is also frequently referred to as PPO (poly(2,6-dimethyl-1,4-phenylene oxide)), especially in the American-Pacific region, as the material was initially commercialised under this name. With regard to PPE in particular, blends of the most significant commercial interest are miscible PPE/polystyrene blends (PPE/PS) and reactively-compatibilised PPE/polyamide blends (PPE/PA). In contrast, blends of PPE and poly(styrene-*co*-acrylonitrile) (PPE/SAN) are expected to provide various advantages, combining the toughness, the flame-retardant behaviour, and the high heat distortion temperature of PPE with the chemical resistance, the low material cost, the resistance to stress cracking, and the high stiffness of SAN.

The miscibility of PPE and SAN is strongly dependent on the composition of SAN, more precisely, on the ratio between styrene and acrylonitrile (AN). Miscibility at all temperatures occurs up to 9.8 wt% of AN in SAN, whereas at higher contents above 12.4 wt%, phase separation occurs. This phase

* Corresponding authors. Tel.: +49 921 55 7470; fax: +49 921 55 7473.
** Tel.: +49 921 55 3399; fax: +49 921 55 3393.
E-mail addresses: altstaedt@uni-bayreuth.de (V. Altstädt), axel.mueller@uni-bayreuth.de (A.H.E. Müller).
[1] Present address: Institute of Polymer Research, GKSS Research Centre Geesthacht, D-21502 Geesthacht, Germany.

0032-3861/$ - see front matter © 2006 Elsevier Ltd. All rights reserved.
doi:10.1016/j.polymer.2006.02.064

separation leads to a two-phase structure, independent of the temperature [3,4]. Intermediate compositions exhibit a lower critical solution temperature behaviour (LCST). Taking into account that SAN copolymers of technical relevance have AN contents between 19 and 35 wt% in order to ensure high chemical resistance compared to PS, such blends with PPE are not miscible and show a coarse morphology. A recent study by Merfeld et al. [4] has verified that the interfacial properties of PPE/SAN blends reflect the AN content. For example, an AN content of 20 wt% leads to an interfacial thickness of only 5 nm which demonstrates the strongly segregated behaviour. As a consequence of the low interfacial thickness and interfacial strength observed for such incompatible blends, the mechanical properties determining the fracture behaviour such as ultimate fracture strain, impact strength and fracture toughness of the blends should be lower than those predicted by the linear rule-of-mixtures.

Earlier works investigating PPE/SAN 40/60 (weight composition) and PPE/ABS 48/52 blends, respectively, support this assumption; blends prepared by both solvent-mediated processing as well as melt-processing showed a brittle behaviour [5–8]. Fekete et al. [9] showed that some mechanical properties such as modulus and strength of PPE/SAN blends can be described by a linear rule-of-mixture approach over a wide range of compositions. These experimental results for melt-blended samples were explained on the basis of a partial miscibility, deduced from observed shifts in the glass transition temperatures of both components by around 2–3 K. However, an earlier study [10] has shown that the presence of low molecular weight components (which are likely present in the used commercial polymers) can lead to similar shifts in the glass transition temperatures of such blends. Using purified materials in their work, Stadler et al. [5] did not report such behaviour for PPE/SAN.

A common approach to improve the toughness of incompatible blends is the chemical or physical compatibilisation [1,2,11]. In the latter case, surface-active block copolymers are often employed to control both the morphology and the resulting physical properties of immiscible blends [12–15]. The addition of block copolymers improves the dispersion due to a reduced interfacial tension and inhibition of collision-induced coalescence [16].

Diblock copolymers (A-*b*-B) with a defined composition have been shown to enhance the dispersion and the load transfer between PPE and SAN; a consequence of the selective entanglement of both end blocks in the interfacial region [4,5,8]. Although the mechanical properties such as stiffness and strength of such compatibilised PPE/SAN blends are significantly improved, the toughness remains insufficient. An efficient way to achieve a significant toughness increase is provided by the use of triblock terpolymers when appropriately composed. In particular, polystyrene-*block*-polybutadiene-*block*-poly(methyl methacrylate) triblock terpolymers (SBM) and their hydrogenated version, poly(styrene)-*block*-poly(ethylene-*co*-butylene)-*block*-poly(methyl methacrylate) are advantageous as a compatibilising agent in PPE/SAN-blends [5,17]. A so-called 'raspberry morphology' of PPE/SAN/SEBM blends was reported by Stadler et al. for the first time [5], which was also found in PPE/SAN/SBM blends [6,7].

This raspberry morphology, obtained by solvent-mediated processing, is schematically shown in Fig. 1. Each end block of the SBM is selectively miscible with one blend component, in particular, an entanglement of PMMA in SAN (miscibility for AN content of 19 wt%) [18,19] and of PS in PPE [20] is observed. The incompatibility of the elastomeric middle block with both the blend components and the end blocks as well as the balanced chemical interaction parameters lead to a discontinuous distribution of PB and PEB spheres, respectively, within the interface. It is important to note that the investigated systems were close to or at thermodynamic equilibrium due to the fact that solvent-mediated processing was employed.

Nevertheless, Lach et al. [6] and Kirschnick et al. [7] have already demonstrated the feasibility of melt-processing of PPE/SAN 40/60 blends using SBM as a compatibiliser. Although the raspberry morphology could be observed, PPE formed the disperse phase in the SAN matrix, independent of SBM composition and processing conditions. In order to further improve the overall behaviour of such compatibilised blends, a continuous PPE phase is desirable, since PPE is the component with the higher glass transition temperature and toughness.

The aim of this study, therefore, was the systematic investigation of the influence of the composition of SBM compatibilisers on the resulting morphology of melt-processed PPE/SAN blends with a weight composition of 60/40. Melt-compounding of the base polymers and compatibilisation by four SBM types with varying block lengths with weight fractions of up to 20 wt% was carried out by twin-screw extrusion, followed by injection-moulding. The morphological features of these blend systems as function of the composition and processing parameters are correlated with the resulting thermal and thermo-mechanical properties. The observations described in this paper provide the necessary basis for a

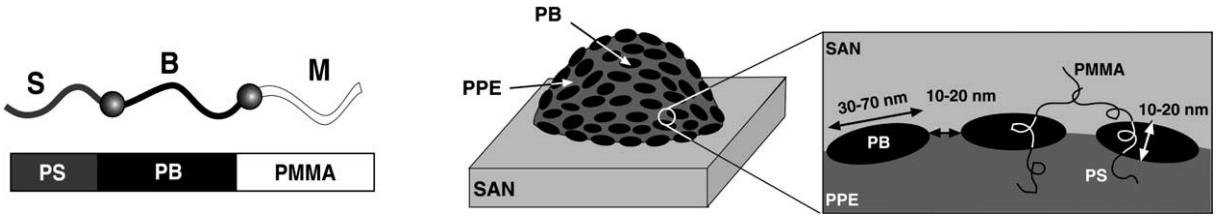

Fig. 1. SBM and model of the 'raspberry' morphology within a PPE/SAN/SBM blend [5].

fundamental evaluation of the resulting mechanical properties of such triblock terpolymer-compatibilised PPE/SAN blends.

2. Experimental

2.1. Materials

The commercial poly(styrene-*co*-acrylonitrile) resin (SAN) used in this study is a copolymer with an acrylonitrile content of 19 wt%, having a weight-average molecular weight M_w = 112 kg/mol and a polydispersity of 1.95. The low acrylonitrile content ensures homogeneous miscibility between SAN and PMMA at the relevant processing conditions [18,19]. In contrast to the SAN in pellet form, non-commercial poly(2,6-dimethyl-1,4-phenylene ether) was obtained as a powder, with a weight–average molecular weight of 12.9 kg/mol and a polydispersity of 1.63. The average molecular weights of SAN and PPE were determined by GPC analysis by an UV detector relative to polystyrene standards at 40 °C, using THF as a solvent. The materials, SAN VLL 19100 and PPE PX100F, were kindly supplied by BASF AG, Ludwigshafen, Germany, and Mitsubishi Engineering Plastics Europe, Düsseldorf, Germany, respectively. Irganox 1010 and Irgafos 168 (Ciba AG) were used as stabilisers.

2.2. Synthesis of SBM triblock terpolymers

Different SBM triblock terpolymers with varying block lengths and a narrow molecular weight distribution were synthesised by sequential anionic polymerisation on a kilogram scale. In contrast to earlier studies of Stadler et al. [21], the synthesis was performed in toluene, leading to the formation of 1,4-, rather than 1,2-polybutadiene as the middle block. 1,4-polybutadiene shows a significant improvement of toughness at low temperatures compared to 1,2-polybutadiene, resulting from the approximately 60 K lower glass transition temperature. Based on earlier studies on the effect of aluminium compounds in the anionic polymerization of MMA in toluene [22–24], the following procedure was used (example: SBM 1) [25].

2.2.1. Reagents

Twenty litre of technical grade toluene were dried over molecular sieves overnight, bubbled with nitrogen for 15 min, and refluxed for 1 day. Then, 7 ml 1,1-diphenylethylene and approximately 100 ml *sec*-butyllithium (1.3 M solution in cyclohexane/hexane 92/8, Acros) were added via syringe, until a red colour persisted. The solvent was refluxed for another 2–3 days and distilled into a purified vessel.

Styrene (BASF) was distilled from CaH_2 under nitrogen, stirred over Bu_2Mg and condensed into storage ampoules. 1,3-butadiene (Rießner Gase) was passed over columns with molecular sieves and activated alumina, followed by storage over Bu_2Mg before use. MMA (BASF) was purified over $AlEt_3$, condensed into an ampoule und stored under nitrogen in the frozen state.

1,2-dimethoxyethane (DME, Merck) was refluxed over potassium for 3 days. After distillation into a flamed bulb it was again degassed.

Within a glove-box, 98 ml (58 mmol) of di[2,6-di(*tert*-butyl)-4-methyl phenoxy]isopropyl aluminium ($iBAl(BHT)_2$ (Nippon Aluminium Alkyls, Ltd, gift of Kuraray Co., Ltd, Japan) were transferred into a flame-dried ampoule. Shortly before the polymerisation, 32 ml purified DME were added.

2.2.2. Polymerisation

A 10 l stainless steel reactor (Büchi), equipped with glass windows, was cleaned with boiling toluene. It was filled with 3.2 l toluene and 1 ml degassed styrene. Then, *sec*-BuLi solution (0.4–0.8 ml) was added dropwise until a slight yellow colour persisted. The solution was brought to 24 °C. 6.3 ml (9.4 mmol) *sec*-BuLi solution were added via syringe. Then 341 ml (2.96 mol) styrene were added and reacted for 80 min. Meanwhile 475 ml (309 g, 5.71 mol) butadiene were condensed into an ampoule that was cooled to −20 °C. After the complete conversion of styrene, a sample was taken for characterisation and the reaction solution cooled to +10 °C. Then butadiene was added. The temperature was stepwise increased to 40 °C. After 160 min a further sample was taken and the solution cooled to −10 °C. First the catalyst/DME mixture was added, then MMA. After 1 h the solution was warmed to 25 °C. The polymerisation was finished after another 220 min and terminated with degassed methanol.

The reaction mixture was diluted with 3 l toluene and extracted with 3 l 2% aqueous H_2SO_4 by rigorous stirring for 1 h (extraction of the catalyst). The organic phase was separated and washed with distilled water to remove residual H_2SO_4. 0.5% BHT (relative to polymer weight) were added as stabiliser and the polymer was precipitated into 50 l isopropanol.

The molecular properties of triblock terpolymers are summarised in Table 1. All molecular weights of the SBM materials were carefully selected to be equal to or above the

Table 1
Composition of the synthesised triblock terpolymers

Triblock terpolymer		M_n (kg/mol)	$M_{n,S}$ (kg/mol)	$M_{n,B}$ (kg/mol)	$M_{n,M}$ (kg/mol)	1,4-B (%)	M_w/M_n
SBM1	$S_{28}B_{36}M_{36}^{105}$	105	29	38	38	90	1.02
SBM2	$S_{33}B_{34}M_{33}^{94}$	94	31	32	31	90	1.02
SBM3	$S_{50}B_{27}M_{23}^{126}$	126	63	34	29	90	1.02
SBM4	$S_{40}B_{20}M_{40}^{90}$	90	36	18	36	89	1.02

The indices denote the composition in weight-%, exponents indicate the number-average molecular weight in kg/mol.

critical molecular mass for entanglements (critical molecular mass of 31.2 kg/mol of polystyrene and 18.4 kg/mol of poly(methyl methacrylate), respectively [26]). With regard to SBM1, SBM2 and SBM3, the weight ratio between polybutadiene and poly(methyl methacrylate) was kept almost constant, whereas the weight content of polystyrene is selected to be either lower, equal or higher than the other blocks, respectively. In SBM4, the weight fraction of the end blocks is balanced; in contrast the amount of the polybutadiene middle block is reduced. After synthesis, the SBM was cryo-ground, in order to achieve a homogeneous distribution of the SBM in the dry-blend with PPE and SAN.

2.3. Melt processing of the blends—extrusion and injection-moulding

Prior to the melt-blending operations, the PPE powder and the SAN pellets were vacuum-dried at 80 °C for 12 h. In contrast, a decreased temperature of 40 °C was selected for the SBM which was further cryo-ground to obtain a powder material. Subsequently, PPE, SAN, and SBM were dry-blended using metered weight contents of the SBM compatibiliser. The ratio between PPE and SAN was held constant at 60/40, the content of SBM was set at 0, 5, 10 and 20 wt%, respectively. Furthermore, 0.1 wt% of a stabiliser (mixture of Irganox 1010 and Irgafos 168) was added to prevent thermal degradation, especially cross-linking of PB and PPE. The final compositions are summarised in Table 2.

The materials were melt-blended using a co-rotating twin-screw extruder (Brabender DSE 20/40) with a screw diameter of 20 mm and a screw length of 600 mm ($L/D = 30$). The maximum barrel temperature and the nozzle temperature were fixed to 250 and 245 °C, respectively. The throughput was kept constant at 1.3 kg/h at a constant screw speed of 50 rpm by volumetric feeding. Consequently, the mean residence time of the blends in the extruder was approximately 5 min. The melt was subsequently quenched in water to avoid thermal degradation and was chopped into pellets. In contrast to earlier studies [7], the processing temperatures were increased by approximately 10 °C, due to the higher amount of highly viscous PPE (60 wt% compared to 40 wt%).

Injection-moulded tensile test specimens with a thickness of 2 mm and a width of 4 mm (according to ISO 527-2) were prepared using an Arburg Allrounder 320S 500-150 machine (screw diameter of 30 mm) at an injection speed of 114 cm^3/s. The maximum barrel temperature was set at 280 °C. The mould temperature was limited to 80 °C in order to guarantee demoulding without deforming the specimens.

Table 2
Composition of the uncompatibilised and the compatibilised blends

PPE	SAN	SBM (according to Table 1)
Uncompatibilised blend		
60	40	–
Compatibilised blends		
57	38	5
54	36	10
48	32	20

Figures denote the composition in wt%. Furthermore, 0.1 wt% of a stabiliser was added.

2.4. Morphological investigations

Ultrathin sections (50 nm) from the processed materials after extrusion and injection-moulding, respectively, were cut at room temperature using an ultra-microtome (Reichert-Jung Ultracut E microtome equipped with a diamond knife). The ultrathin sections were stained using OsO_4 and RuO_4 as previously described [5,7,21,27]. Due to this particular staining method, SAN and PPE appear as the bright and the dark phase, respectively, whereas the PB block of the SBM is selectively stained by OsO_4 and appears black. Bright field transmission electron microscopy at an acceleration voltage of 80 kV was carried out using a Zeiss 902 TEM.

2.5. Rheological investigations

Dynamic shear experiments were performed using a Rheometrics Dynamic Analyser RDA III in the plate-plate configuration with a plate diameter of 25 mm and a gap of 1 mm. The storage modulus, the loss modulus, and the complex viscosity of PPE and SAN, respectively, were measured as a function of frequency in the range of 0.01–500 rad/s at 260 °C. Prior to each measurement, the linear viscoelastic region was determined by carrying out an amplitude sweep at a deformation of 0.1–100%, at a frequency of 1 rad/s. Subsequently, the deformation of the frequency sweeps was set to be within the linear viscoelastic region.

2.6. Thermal and dynamic mechanical thermal analysis

Differential scanning calorimetry (DSC) of the blends was conducted using a Mettler DSC/SDTA 821e, calibrated using indium and zinc standards. Specimens of 8–10 mg were taken form the pelletised blends after extrusion and from the centre of the injection-moulded test specimens. The samples were subjected to a heat–cool–heat cycle between 25 and 250 °C under nitrogen atmosphere. A heating rate of 20 K/min was selected to investigate the glass transitions; in contrast, a lower cooling rate of 10 K/min after the first heating was chosen to ensure a controlled and slow cooling of the sample in comparison to the fast cooling rates experienced during melt-processing. In order to reduce the experimental error and to analyse the homogeneity of the materials, three measurements were carried out for each blend. Due to the width of the observed glass transitions, the glass transition temperatures were taken as the maximum of the differentiated heat flow.

The dynamic mechanical thermal analysis (DMTA) of the blends was performed in the dual-cantilever mode (specimen dimensions of 20 mm × 4 mm × 2 mm) using a Mettler Toledo DMA/SDTA 821e at a constant frequency of 1 Hz. The applied strain was kept small enough to ensure linear-elastic behaviour of all systems. After equilibration at −100 °C, the temperature

was continuously increased to a maximum of 240 °C at a heating rate of 2 K/min.

3. Results and discussion

3.1. Morphology of SBM triblock terpolymers

Triblock terpolymers are copolymers consisting of three blocks of chemically different constituents and they can show a manifold variety of different phase morphologies. The phase behaviour depends both on the interaction parameters between the respective components, on the respective block lengths as well as on the sequence of the blocks [28]. Significant scientific attention has been focussed on the investigation of the morphology of SBM triblock terpolymers, especially by Stadler and his group [5,21,29]. The morphologies of these rather strongly microphase-separated systems were mainly studied at room temperature following casting from solution, slow removal of the solvent and, finally, annealing at elevated temperatures. Due to this already existing detailed analytical description, the morphology of the SBM materials used in this study is briefly reviewed here and compared to the present morphologies.

The phase diagram of SBM and the observed morphologies as a function of the composition are shown in Fig. 2. The regions labelled as 'll', 'lc' and 'u-cc/cc' indicate typical morphologies as observed by Stadler et al. [5,21,29] and are in good agreement with the present triblock terpolymers. The abbreviation 'll' (lamella–lamella) denotes morphologies with lamellas of PS, PB as well as PMMA and was verified for block copolymers of both SBM1 ($S_{28}B_{36}M_{36}^{105}$) and SBM2 ($S_{33}B_{34}M_{33}^{94}$) with nearly equal amounts of each constituent. The continuous increase of the block length of PS leads to the following morphological arrangement: PS appears as the matrix and PMMA forms cylinders which are covered by a PB shell (cylinder–cylinder, 'cc'). With regard to SBM3 ($S_{50}B_{27}M_{23}^{126}$), this particular composition is located in the transition region between 'll' and 'u-cc/cc' (undulated cylinder–cylinder/cylinder–cylinder, 'u-cc/cc'). Returning to symmetric SBM triblock terpolymers such as SBM2, the reduction of the PB content and the equal block lengths of PS and PMMA lead to the formation of cylinders of PB at a lamellar PS/PMMA interface (lamellar–cylinder, 'lc'). This morphological arrangement is also found and verified for SBM4 ($S_{40}B_{20}M_{40}^{90}$).

These morphologies of the pure SBM materials will be used in the following sections to discuss their efficiency to act as a compatibiliser in a PPE/SAN blend. On the one hand, the block lengths of the respective SBM materials were carefully selected in order to ensure entanglement and thus sufficient molecular mixing with the blend components (according to earlier studies, the critical entanglement molecular weights of PS and PMMA were assumed as 31.2 and 18.4 kg/mol, respectively, [26]). On the other hand, a low molecular weight of the SBM materials ensures a low viscosity of the block copolymer and thus allows a good dispersion during melt-compounding. As a result, the finally selected molecular weight was relatively low (around 100 kg/mol).

3.2. Rheology and prediction of the morphology of uncompatibilised blends

The morphology of immiscible polymer blends is strongly influenced by the rheological properties of the base polymers, in the present case PPE and SAN. As the uncompatibilised blend forms the starting point for the interfacial modification by SBM, a more detailed investigation of the correlation between morphology development and melt properties of this particular system is reasonable. The prediction of the phase inversion region, where both SAN and PPE form continuous phases, is often taken as a first indication of the resulting blend morphology [1,2]. Starting from the co-continuous morphology, an increasing SAN content leads to the formation of a dispersed PPE phase embedded in the SAN matrix. However,

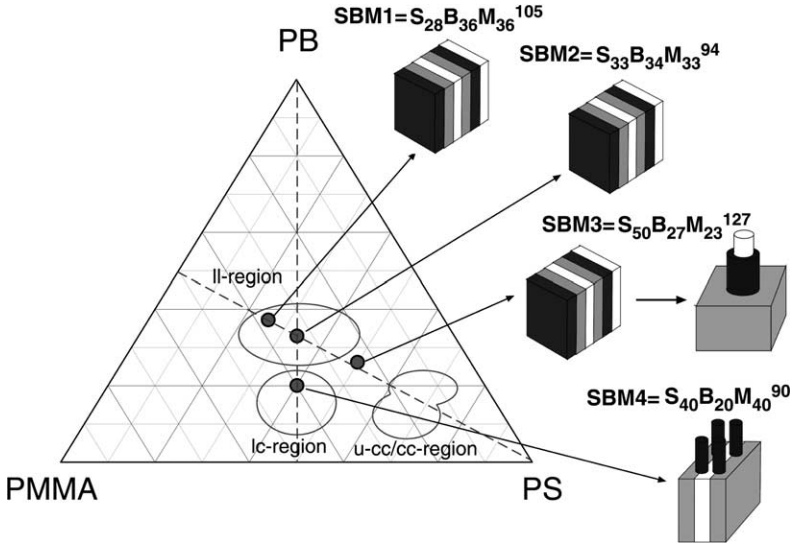

Fig. 2. Morphologies of pure SBM triblock terpolymers following solvent-mediated processing (in accordance with [30]; PS, dark; PB, black; PMMA, white).

the phase inversion point depends on various parameters, in particular, the viscosity ratio which denotes the ratio between the respective viscosities of the dispersed phase and the matrix.

The magnitude of the complex viscosities of PPE and SAN as a function of shear rate at a processing-relevant temperature of 260 °C is shown in Fig. 3. Typical shear rates of lab-scale and large-scale extrusion processes are 50–500 s^{-1} [30,31]. The results demonstrate that the viscosity of PPE is significantly higher than that of SAN over the whole shear rate regime encountered during processing. The resulting viscosity ratio for this particular blend system as a function of shear rate is shown in Fig. 4.

Subsequently, the empirical model of Jordhamo et al. [32], based on the viscosity ratio and the volume fraction ϕ of the respective phases, allows the prediction of the phase inversion region (Eq. (1)):

$$\frac{\eta_{PPE}}{\eta_{SAN}} = \frac{\phi_{PPE}}{\phi_{SAN}} \tag{1}$$

Following this empirical approach, the volume fraction of PPE must be significantly higher than the volume fraction of SAN in order to achieve a co-continuous morphology. However, this model often fails to predict the phase inversion region correctly for blends with a large viscosity mismatch as in the present case. Here, the outcome of this model is an overestimation of the necessary volume fraction of the high viscous PPE phase. More accurate models should be applied, e.g. the approach proposed by Chen and Su [33] (Eq. (2)):

$$\frac{\phi_{PPE}}{\phi_{SAN}} = 1.2\left(\frac{\eta_{PPE}}{\eta_{SAN}}\right)^{0.3} \tag{2}$$

Alternatively, a model based on the emulsion theory was developed by Utracki [34] (Eq. (3)):

$$\frac{\eta_{PPE}}{\eta_{SAN}} = \left(\frac{\phi_m - \phi_{SAN}}{\phi_m - \phi_{PPE}}\right)^{[\eta]\phi_m} \tag{3}$$

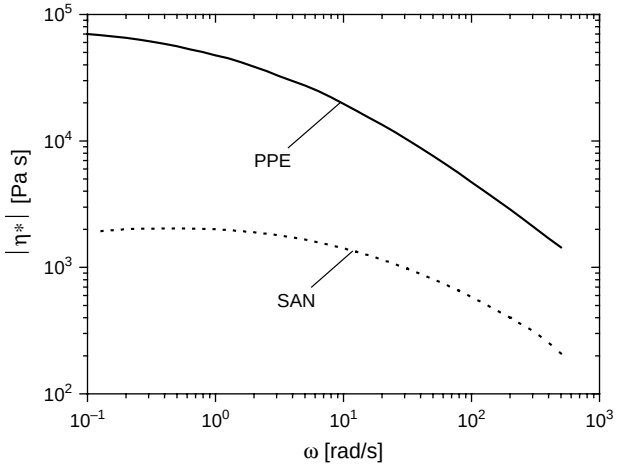

Fig. 3. Magnitude of the complex viscosities of the base materials PPE and SAN, respectively.

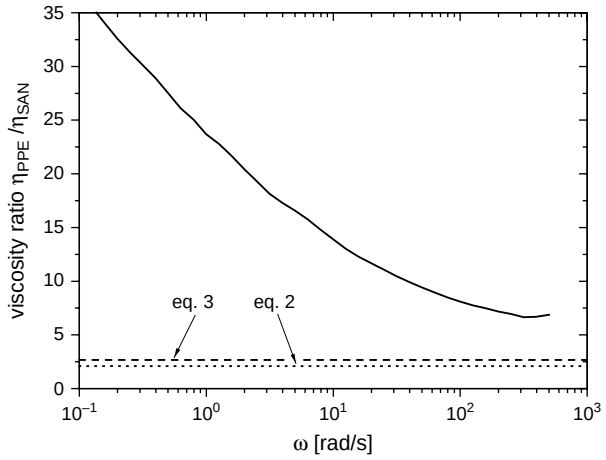

Fig. 4. Prediction of the phase inversion point. The full line shows the experimental viscosity ratio of PPE to SAN, respectively, at a temperature of 260 °C. Dashed and dotted lines denote theoretical predictions for the viscosity ratio at which phase inversion of a PPE/SAN 60/40 blend should occur. An SAN matrix is assumed due to the higher experimental viscosity ratio.

Here, the parameter ϕ_m as the maximum packing volume fraction is calculated from $\phi_m = 1 - \phi_c$, where ϕ_c denotes the onset of phase continuity. Furthermore, the exponent $[\eta]$ represents the dimensionless intrinsic viscosity as described elsewhere [34]. For most polymer blends, the following parameters are in good agreement with experimentally observed morphologies: $[\eta] = 1.9$ and $\phi_m = 0.84$ [2].

Using Eqs. (2) and (3), the viscosity ratios necessary to obtain phase inversion of a PPE/SAN 60/40 blend can be calculated and compared to the experimentally determined values (see dashed and dotted lines in Fig. 4). As the theoretically predicted ratios of 2.1 and 2.6, respectively, are significantly lower than the experimental values over the whole range of shear rates, blends with an SAN matrix are expected for the selected processing conditions.

According to these considerations, a PPE matrix, which is favourable with regard to the thermal and mechanical properties of this blend system, can only be achieved at higher contents of PPE (approximately 70 wt%). On the other hand, independent of blend composition and resulting phase morphology, a suitable compatibilisation for PPE/SAN is necessary in order to ensure a sufficient toughness of the final blend. As shown previously [5,6], triblock terpolymers can lead to this desired increase in toughness of PPE/SAN blends; however, the thermal stability of the selected SBM compatibilisers [35] limits the processing temperatures and therefore, prevents the use of PPE contents significantly exceeding 60 wt% required for phase inversion.

3.3. Morphology of blends following extrusion

Indeed, the detailed transmission electron microscopy investigations of the uncompatibilised blends verify the theoretically predicted morphology. The TEM image shown in Fig. 5(a) highlights the continuous nature of the SAN matrix

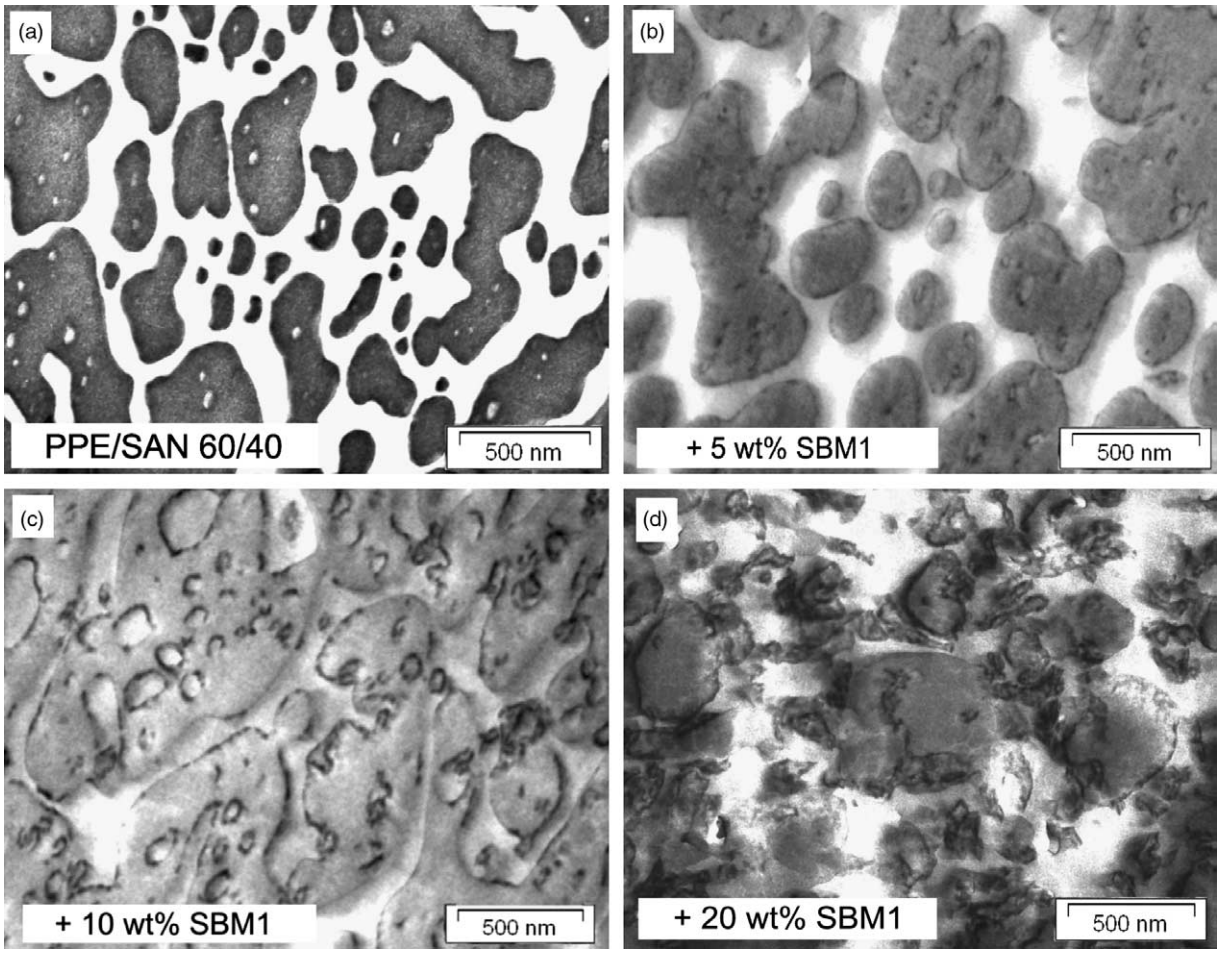

Fig. 5. TEM micrographs of melt-processed PPE/SAN blends following extrusion—uncompatibilised blend and influence of compatibilisation by various amounts of SBM1 on morphology ($S_{28}B_{36}M_{36}^{105}$). (SAN bright, PPE dark, PB midblock of SBM black).

(bright phase). Nevertheless, the PPE (dark phase) does not appear fully dispersed but tends to form more complex continuous particles. This behaviour is not surprising, taking into account that the continuity of the PPE phase does not increase abruptly at the phase inversion region, but rather develops continuously, a typical phenomenon for polymer blends [2]. Although no co-continuous morphology can be observed, the degree of continuity of the PPE phase is expected to be beneficial for the resulting properties of this particular blend.

Compatibilisation of this immiscible PPE/SAN blend by SBM increases the number of possible morphological arrangements, as shown in the pioneering work by Stadler et al. [5]. The thermodynamically stable situation, i.e. the location of the block copolymers at the interface between PPE and SAN is assumed as a reference state. The thermodynamic equilibrium results form the interaction parameters, summarised for the materials used in this study in Table 3. Due to the fact that negative interaction occurs both between PPE/PS and SAN/PMMA, the PMMA block subsequently should extend into the SAN phase whereas PS blocks should extend into the PPE phase. With regard to the interaction parameters between the other components, no further miscible polymer pairs are found and as a result, the 'raspberry morphology' is formed.

However, the morphology of such compatibilised blends following melt-processing can significantly differ from the equilibrium case which is obtained after solvent-mediated processing [6,7]. Evaluating recent studies, the effect of micelle formation following melt-blending is not negligible and is included in the following considerations concerning the possible morphological arrangements of SBM in the melt-processed PPE/SAN 60/40 blends, as schematically shown in

Table 3
Segmental interaction parameters, χ, between the blend components

	PPE	SAN	PS	PB[a]
PPE	0			
SAN	0.034[b]	0		
PS	−0.044 [4]/−0.1 [5]	N.a.	0	
PB[a]	N.a.	N.a.	0.045 [21]	0
PMMA	0.5 [5]	−0.008 [5]	0.0044 [21]	0.071 [21]

[a] Segmental interaction parameters reported for 1,2-PB.
[b] Calculated at 140 °C based on [4].

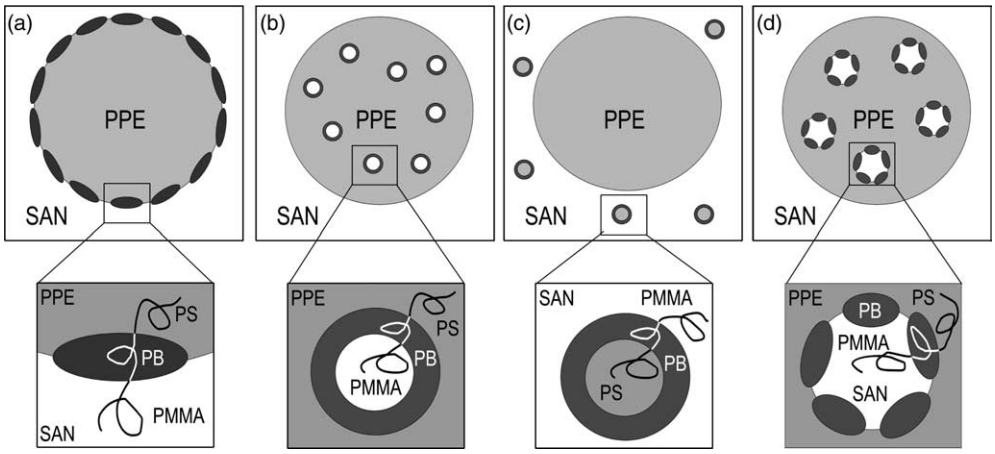

Fig. 6. Possible morphological arrangements of melt-processed PPE/SAN blends containing SBM triblock terpolymers (a) SBM at the interface between PPE and SAN (raspberry morphology) (b) SBM micelles in PPE, whereas the core of the micelles is formed by PMMA; therefore, no interaction with SAN occurs (c) SBM micelles in SAN, whereas the core of the micelles is formed by PS; therefore, no interaction with PPE (d) more complex core–shell particles in the PPE phase; the core is formed by SAN and PMMA, whereas PB is shown as the shell and, finally, the PS block entangles with PPE.

Fig. 6. Based on the previously mentioned TEM observations regarding the uncompatibilised blend, SAN is assumed to always be the continuous phase.

Starting from the equilibrium situation with SBM at the interface (Fig. 6(a)), micellation of SBM can either occur in PPE (Fig. 6(b)) or in SAN (Fig. 6(c)). Furthermore, core–shell particles can be formed in both phases, e.g. SAN particles covered by SBM located in the PPE phase (Fig. 6(d)). In this case, the core of the particles consists of SAN and PMMA, surrounded by a PB layer. Finally, the PS block is entangled with the surrounding PPE. This morphological arrangement is similar to Fig. 6(a), but the interfacial curvature is inverse.

3.3.1. Variation of the SBM content

The morphologies of compatibilised PPE/SAN blends containing an increasing weight fraction of SBM1 following extrusion are shown in Fig. 5(b)–(d). Due to the staining conditions, the PB middle block of SBM appears black. Obviously, the addition of 5 wt% of SBM1 leads to no significant morphological changes as compared to the uncompatibilised 60/40 blend. SAN still forms the continuous phase and the size of the dispersed PPE phase remains unchanged. As in Fig. 5(a), small inclusions of SAN are found in the PPE phase; however, their size is slightly increased due to the SBM. The compatibiliser is mainly located at the interphase, as indicated by the irregularly contrasted regions at the phase boundary. This behaviour is characteristic of the 'raspberry morphology', although not the complete interphase is covered by the ellipsoid PB domains. This difference to morphologies observed for solution-processed samples most likely is a result of the average particle size given by the melt processing and the limited amount of SBM available to cover the particle surface.

Further enrichment of SBM at the phase boundary is observed at 10 wt% of block copolymer. Moreover, the overall morphology of the blend is altered and reveals a co-continuous character which is attributed to a combination of the following two effects: as the number and size of the core–shell particles within the PPE phase increases, the apparent PPE content (PPE plus inclusions) increases. In turn, this effect decreases the viscosity of the PPE phase during processing [7]. As discussed before, both the increased PPE content as well as the reduced viscosity mismatch enhances the development of a continuous PPE phase. Similar results were observed for (PPE/PS)/PP and (PPE/PS)/POM blends [36,37].

Surprisingly, further addition of SBM1 (in total 20 wt%) changes the morphology again to a dispersed PPE phase; however, the phase size of the PPE is reduced in comparison to all previously discussed blends. This change in morphology is attributed to a reduced interfacial tension and limited coalescence of PPE and SAN due to the fact that SBM is present at nearly the complete interface which is indicated by the coverage of the dispersed PPE phase by the triblock terpolymer [16]. Furthermore, inclusions are found in the SAN which do not appear to be core–shell particles due to their dimensions but rather micelles of SBM. This micelle formation is attributed to the saturated coverage of the PPE interface by the block copolymer, preventing further interfacial enrichment. The darker core (polystyrene [1,27]) of these micelles within the SAN strongly implies that the PS block and the PB block are still covalently bound, therefore, verifying that the shear forces and thermal loads have not induced thermal degradation of the SBM during extrusion.

3.3.2. Variation of the length of the PS block

In the following section, a comparison of the final blend morphologies following extrusion as a function of the PS block length is presented and discussed. In order to ensure a sufficient amount of compatibiliser to cover the whole interphase, this comparison is made on blends containing 20 wt% of SBM. In comparison to the previously discussed SBM1 (28 wt% PS), the block length of polystyrene was increased, whereas the ratio between PB and PMMA was kept nearly constant. In contrast to the symmetric SBM2 (33 wt% PS) with equal block

lengths, the polystyrene content of SBM3 (50 wt% PS) is significantly increased.

As in the case of the SBM1, Fig. 7(a), the addition of 20 wt% of the symmetric SBM2, Fig. 7(b), results in a continuous SAN matrix with the block copolymer completely present at the interface. However, no micelles are detected. The peculiar structure of the boundary with regular indents of PB indicates the 'raspberry morphology'. However, a further increase of the PS block length using SBM3, Fig. 7(c), leads to a completely different morphology. A distinct micelle formation has occurred in the PPE phase, with the cores of the micelles consisting of pure PMMA, as indicated by the dimensions of the micelles. Furthermore, PMMA is not stained by RuO_4 and OsO_4 [1,21,27] and, thus, appears relatively bright. Again, the presence of these SBM micelles indicates a sufficient stability of the PMMA and its chemical bonds to PB in the SBM during the selected processing conditions. Although SBM3 is also found at the interface to SAN, the compatibilisation efficiency is low, as most of the SBM is entrapped in the PPE phase. Due to the long PS block, the segmental swelling of PS in PPE is increased and favours the formation of micelles in PPE, an effect that is also known as emulsification failure [38].

As a result of the above outlined experimental observations, a correlation between the composition of SBM and the resulting morphology of the melt-processed blends can be established. Different SBM block lengths lead to a variation of the morphology of the pure triblock terpolymer. In turn, this starting morphology of the compatibiliser strongly affects the efficiency of the triblock terpolymer to compatibilise PPE/SAN blends. For this particular blend system, the length of the PS block of the SBM especially determines the swelling power [21] and subsequently the location of the compatibiliser. High PS contents of the SBM induce the formation of micelles in the PPE phase, whereas equal lengths of the end blocks lead to a balanced swelling in the respective phases and, thus, favour the formation of the raspberry morphology.

As discussed in the context of the uncompatibilised PPE/SAN blend, the entrapment of SBM in the PPE both reduces the viscosity and increases the apparent phase content. Similar effects were discussed for other blend systems, in particular for ternary blends of (PPE/PS)/POM and (PPE/PS)/PP [36,37]. In summary, the location of SBM triblock terpolymers not only affects the compatibilisation efficiency but also the overall morphology development of the blend.

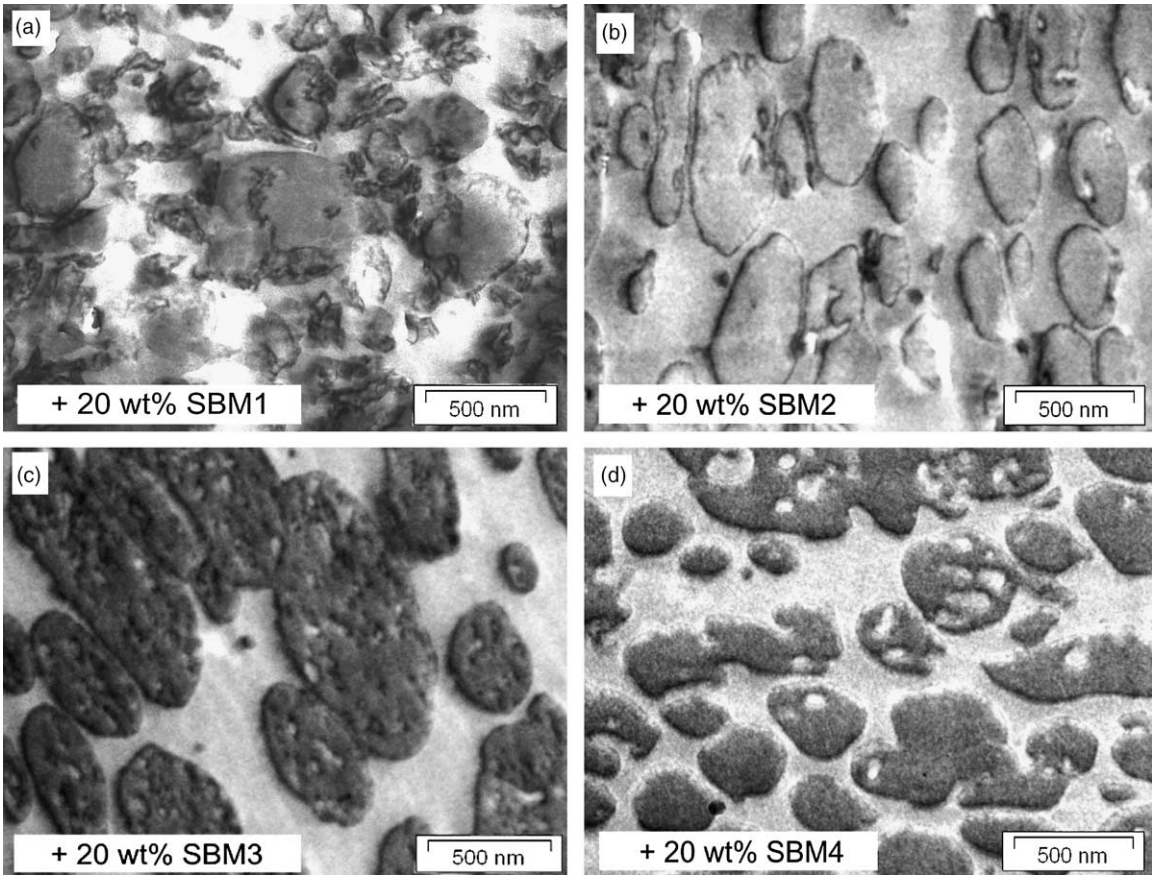

Fig. 7. TEM micrographs of melt-processed PPE/SAN blends following extrusion and compatibilisation by 20 wt% SBM—influence of different SBM materials on compatibilisation (SBM1 = $S_{28}B_{36}M_{36}^{105}$, SBM2 = $S_{33}B_{34}M_{33}^{94}$, SBM3 = $S_{50}B_{27}M_{23}^{126}$, SBM4 = $S_{40}B_{20}M_{40}^{90}$; SAN bright, PPE dark, PB midblock of SBM black).

3.3.3. Variation of the length of the PB block

So far, the influence of the elastomeric middle block on the morphology development of the compatibilised blends has been neglected. Nevertheless, a decreasing PB block length is expected to enhance the mobility of the SBM end blocks. In the extreme case of the PB block diminishing completely, the behaviour of a diblock SM compatibiliser is approached.

In comparison to SBM2 (34 wt% PB), the PB block length of SBM4 (20 wt% PB) is reduced while the length of the two end blocks remains constant. The TEM image in Fig. 7(d) shows, that this reduction in the elastomeric middle block length leads to a similar overall morphology of the blend revealing a continuous SAN matrix. However, an increasing amount of core–shell particles in the PPE is observed which can be attributed to the lower PB content.

3.4. Correlation between blend morphology and thermal properties

The microscopic characterisation of the resulting blend morphology as a function of composition, SBM type and content presented so far allows a first estimation of the resulting solid-state properties of these systems. Nevertheless, a detailed thermal analysis of the various blends should further enhance the understanding of the extent of interfacial mixing at the same time as providing a more macroscopic evaluation of the blend characteristics.

3.4.1. Theoretical consideration of the glass transition behaviour

In the ideal case, the block copolymer should be located at the interface of the PPE and SAN domains. As PPE is homogeneously miscible with PS homopolymers, binary PPE/PS blends show only one glass transition [1,39]. The same principle accounts for blends of SAN (AN-content of 19 wt%) and PMMA homopolymers [19]. In contrast to such homopolymers, both PMMA and PS are chemically bound in the SBM triblock terpolymers, an effect that limits the intimate mixing of the phases. Both the width of the glass transition region as well as the exact value of the glass transition temperature are useful indicators of the degree of interfacial mixing.

In order to achieve an intimate mixing between the end blocks of the block copolymer and the blend components and, subsequently, an efficient mechanical coupling, the so-called wet brush situation is favourable [5]. The negative enthalpic interaction between PPE/PS and PMMA/SAN is thermodynamically favourable and ensures interpenetration. In addition, a block length of the respective SBM end blocks above the critical entanglement molecular weight is essential. For the investigated SBM types, a sufficient molecular weight of the end blocks is provided and, thus, an improved phase adhesion can be assumed as a result of the wet brush situation.

Furthermore, the homogeneity of segmental mixing is limited by the restriction of junction points in the interfacial region, as a result of the chemical links connecting the blocks in the triblock terpolymer. The interaction of the end blocks, forming brushes with the blend components, is expected to be influenced by both the molecular weight of the blocks as well as the degree of dispersion. The influence of both factors on the resulting glass transition of the PPE is schematically outlined in Fig. 8. In Fig. 8(a), the length of the PS blocks is small compared to the PPE phase size. Therefore, no intimate mixing occurs resulting in a dry brush situation, i.e. PS is only present in the interfacial region of the PPE phase and the resulting narrow glass transition is dominated by the inner core region of pure PPE.

With decreasing phase size as a result of improved dispersion, Fig. 8(b), the resulting glass transition behaviour becomes broader and shifts to lower temperatures, reflecting a concentration gradient of PS within the PPE. However, similar features are obtained for an increasing block length at a constant phase size (Fig. 8(c)). Uniform mixing of both phases occurs as a result of long PS blocks with respect to the PPE phase size, both as a result of the decreasing PPE phase size by improved mixing efficiency, Fig. 8(d), as well as a further increasing PS block length, Fig. 8(e). Both effects again decrease the width of the glass transition and reveal a glass transition temperature at a lower value.

In reality, the glass transition behaviour of a polymer blend further depends on the phase size distribution, i.e. broad PPE phase size distributions at a constant PS block length include cases 8a to 8c mentioned above and thus result in broad glass transitions observed experimentally.

The unrestricted and homogeneous mixing of the PMMA blocks with SAN and the PS blocks with PPE is selected as a reference state for theoretical predictions of the resulting glass transition temperature T_g of the respective phases. As shown in earlier studies, the composition dependence of the glass transition temperature of binary PPE/PS blends can be described by the Couchman equation (Eq. (4)) [39]:

$$\ln\left(\frac{T_g(\mathrm{PPE/PS})}{T_g(\mathrm{PS})}\right) = \frac{w(\mathrm{PPE})\Delta c_p(\mathrm{PPE})\ln(T_g(\mathrm{PPE})/T_g(\mathrm{PS}))}{w(\mathrm{PS})\Delta c_p(\mathrm{PS}) + w(\mathrm{PPE})\Delta c_p(\mathrm{PPE})} \tag{4}$$

where w, Δc_p denote the component weight fraction and the change of the heat capacity at the glass transition, respectively. From the literature, $\Delta c_p(\mathrm{PPE}) = 0.221$ J/g and $\Delta c_p(\mathrm{PS}) = 0.281$ J/g [39] can be obtained.

In the case of binary SAN/PMMA blends, the Fox equation [19] is suitable to describe the composition dependence of the glass transition temperature (Eq. (5))

$$\frac{1}{T_g(\mathrm{PMMA/SAN})} = \frac{w(\mathrm{PMMA})}{T_g(\mathrm{PMMA})} + \frac{w(\mathrm{SAN})}{T_g(\mathrm{SAN})} \tag{5}$$

The measured glass transition temperatures of the different SBM materials are summarised in Table 4, in order to provide a base for the theoretical prediction of the glass transition temperature of the respective blend phases. Experimental error is approximately 1 K.

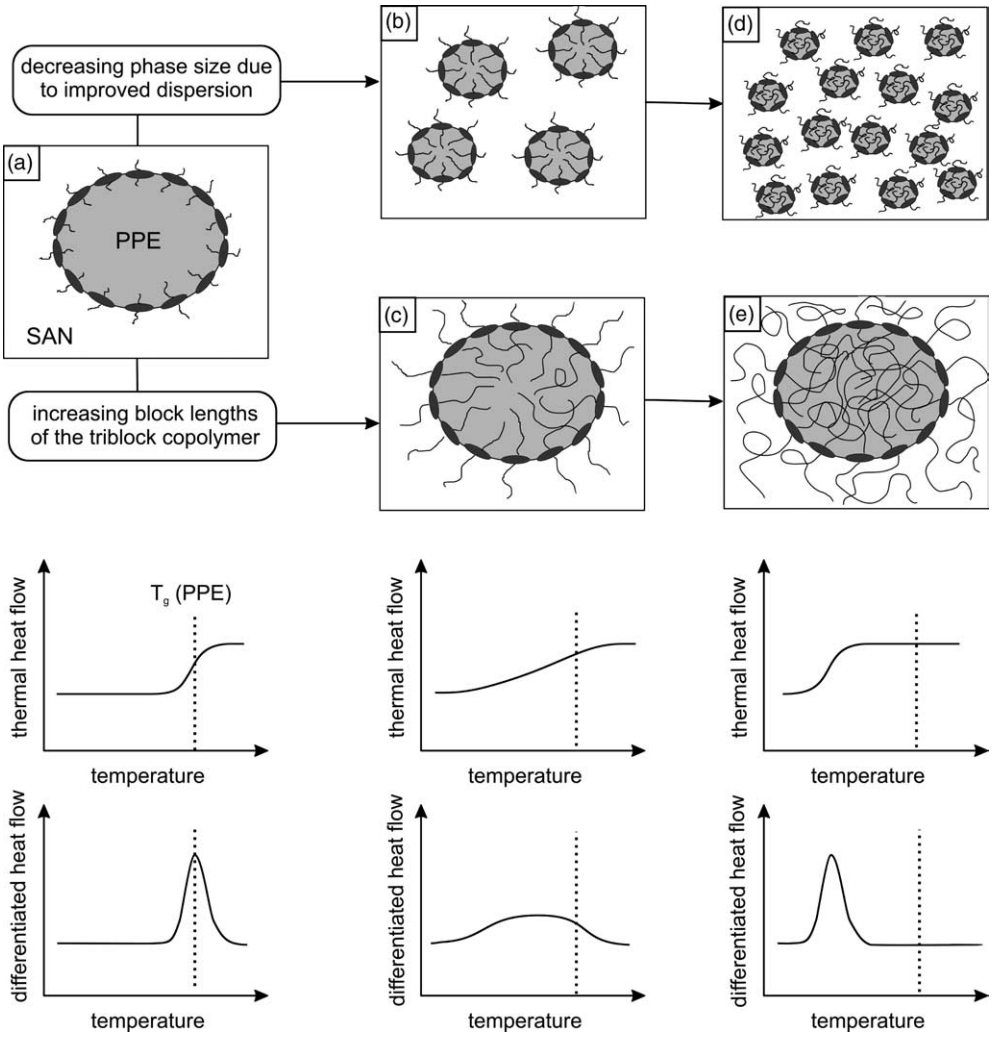

Fig. 8. Schematic representation of the interfacial situation and segmental mixing in PPE/SAN/SBM blends and their influence on the glass transition behaviour of the respective phases.

As a result of the large difference in glass transition temperature between PPE (~216 °C) and PS (~105 °C), the glass transition temperature obtained after blending of both polymers is very sensitive with regard to the blend composition and the degree of interfacial mixing. In contrast, the difference in glass transition temperature between SAN (~114 °C) and PMMA (~131–135 °C) is rather small and the increase in the glass transition temperature of SAN after addition of SBM is less distinct.

For example, considering the ternary blend with the largest content of PMMA (PPE/SAN/SBM1 48/32/20), the expected shift of the glass transition temperature of SAN is on the order of 3 K, assuming homogeneous mixing of both phases. With regard to the other blends, the increase in T_g is even smaller and approaches the experimental error. Therefore, the average T_g value including error bars of three measurements on each blend system is reported (Fig. 10). For comparison, the thermal features observed during the first and second DSC heating cycle were recorded; however, no differences were observed.

3.4.2. Experimental results of the blends following extrusion

Typical DSC traces for the uncompatibilised PPE/SAN blend as well as the blend with increasing weight fraction of SBM4 are shown in Fig. 9 as an example. The uncompatibilised blend shows two distinct glass transition temperatures at 114 °C (SAN) and 216 °C (PPE). Following melt-blending, a shift of the T_g of the pure components of up to 1–3 K was observed, in agreement with data presented in Ref. [9]. As we will focus on the influence of SBM on the thermal features, the

Table 4
Glass transition temperatures, T_g, of the base materials as obtained by DSC at a heating rate of 20 K/min

Material		T_g (°C)
SAN		114
SBM1	$S_{28}B_{36}M_{36}^{105}$	102 (PS), 131 (PMMA)
SBM2	$S_{33}B_{34}M_{33}^{94}$	104 (PS), 132 (PMMA)
SBM3	$S_{50}B_{27}M_{23}^{126}$	109 (PS), 132 (PMMA)
SBM4	$S_{40}B_{20}M_{40}^{90}$	107 (PS), 135 (PMMA)

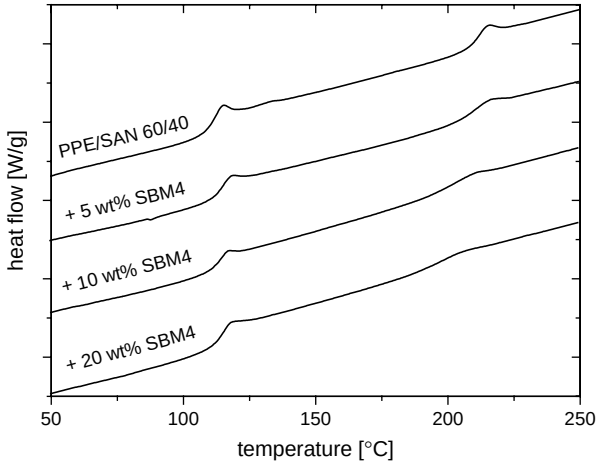

Fig. 9. DSC curves of uncompatibilised PPE/SAN blend and after compatibilisation by various amounts of SBM4 ($S_{40}B_{20}M_{40}^{90}$) following melt-compounding. Curves show the endothermic heat flow obtained at the second heating cycle and are shifted for a better comparison.

blended state of PPE and SAN is used as a reference and for the calculations of the glass transition temperatures of the compatibilised blends. The degree of miscibility will be discussed in a further paper in correlation with the mechanical properties.

Returning to Fig. 9, the glass transition temperature of the PPE is significantly reduced with increasing weight fraction of SBM4, even for small contents of SBM4. This effect is due to the interpenetration of the PS block into the PPE. Furthermore, a significant broadening of the glass transition is observed, indicating a large segment density gradient of PS in the PPE phase. This explanation appears reasonable, as the PPE particle size distribution is relatively broad and the dimensions of the PS block are smaller than the phase size of PPE. Although enthalpic driven stretching occurs [5], the PS concentration within a PPE particle remains inhomogeneous. As a result of the small difference in glass transition temperature between PMMA and SAN, the shift is not well seen in Fig. 9—however, a broadening of the SAN transition towards higher temperatures is observed. This observation, again, is an indication of the segment density gradient in SAN.

Fig. 10 summarises the glass transition temperatures for the various PPE/SAN/SBM blends following extrusion (open symbols). The dotted line represents the homogeneously mixed states of the end blocks of SBM with the respective phases of the blend, calculated according to Eqs. (4) and (5). The data shown in Fig. 10(a) for the blend compatibilised with SBM1 are in reasonable agreement with the morphological arrangements discussed in Section 3.3.1. Independent of content of the triblock terpolymer, the PMMA block interpenetrates into the SAN phase, increasing the glass transition temperature of SAN in agreement with the theoretical predictions. Due to the fact that the glass transition is broadened, a concentration gradient of the entangled PMMA phase in the SAN can be assumed. For low contents of SBM1, a similar behaviour is demonstrated for the segmental mixing of PS and PPE; however, at higher contents of approximately 10 wt% of SBM1, the decrease in glass transition temperature levels off. This effect reflects the saturation of the PPE interface and the associated micelle formation in SAN, so that PS blocks with no interpenetration exist. Subsequently, an additional glass transition of PS should occur. However, DSC allows no detection of this transition due to the small contents of PS (maximum 6 wt%) and due to the partial overlap with the glass transition of SAN.

Previously, the high compatibilisation efficiency of SBM2 was demonstrated by the TEM images showing the butadiene block at the interface, even at high SBM contents of 20 wt%. This behaviour is reflected by the shifts of the glass transition temperatures of both PPE and SAN which closely follow the theoretically predicted shifts, independent of SBM content (Fig. 10(b)). This agreement indicates an efficient mixing of the end blocks with the respective phases. As a result of the inhomogeneous particle size and the relatively short block lengths compared to the phase size relatively broad glass transitions are observed, in agreement with other studies [40]. Similar glass transition broadenings are observed for all SBM types and contents.

However, closer inspection of the thermal features of the blends containing SBM3 reveals further characteristic aspects (Fig. 10(c)). The glass transition temperature of SAN shows no increase after addition of 5 wt% of SBM3. Although higher SBM contents lead to a small shift to higher temperatures, the theoretically predicted values are not reached. In contrast, the corresponding glass transition temperature of the PPE phase reflects rather good agreement with the model. This particular behaviour indicates micelle formation in the PPE already at low contents of SBM3, whereas at higher contents, both micelles in the PPE and a partial location of SBM3 at the phase boundary between PPE and SAN are indicated. These explanations correlate with the TEM observations.

Finally, SBM4 shows good segmental mixing between PPE and PS; however, the SAN glass transition appears to deviate from the theoretical prediction. This behaviour is not expected, considering the previously discussed morphological features. The broadening of the glass transition of SAN towards the T_g of PMMA ($\sim$135 °C) can be related to a significant segmental density gradient. Although closer analysis of the DSC traces at the relevant temperature range provides clear evidence for the presence of a high-temperature shoulder, the chosen evaluation method (maximum of the differentiated heat flow) does not fully take into account this high-temperature feature. The values plotted in Fig. 10(d), therefore, present an underestimation of the true glass transition temperature of the homogeneous SAN/PMMA blend.

3.4.3. Prediction of the morphology of injection-moulded specimens based on DSC

In summary, a correlation between the thermal properties and the morphological arrangements of the various blends under investigation following melt-compounding can be established. These correlations can now be used to predict the final morphology of the injected-moulded specimens. In

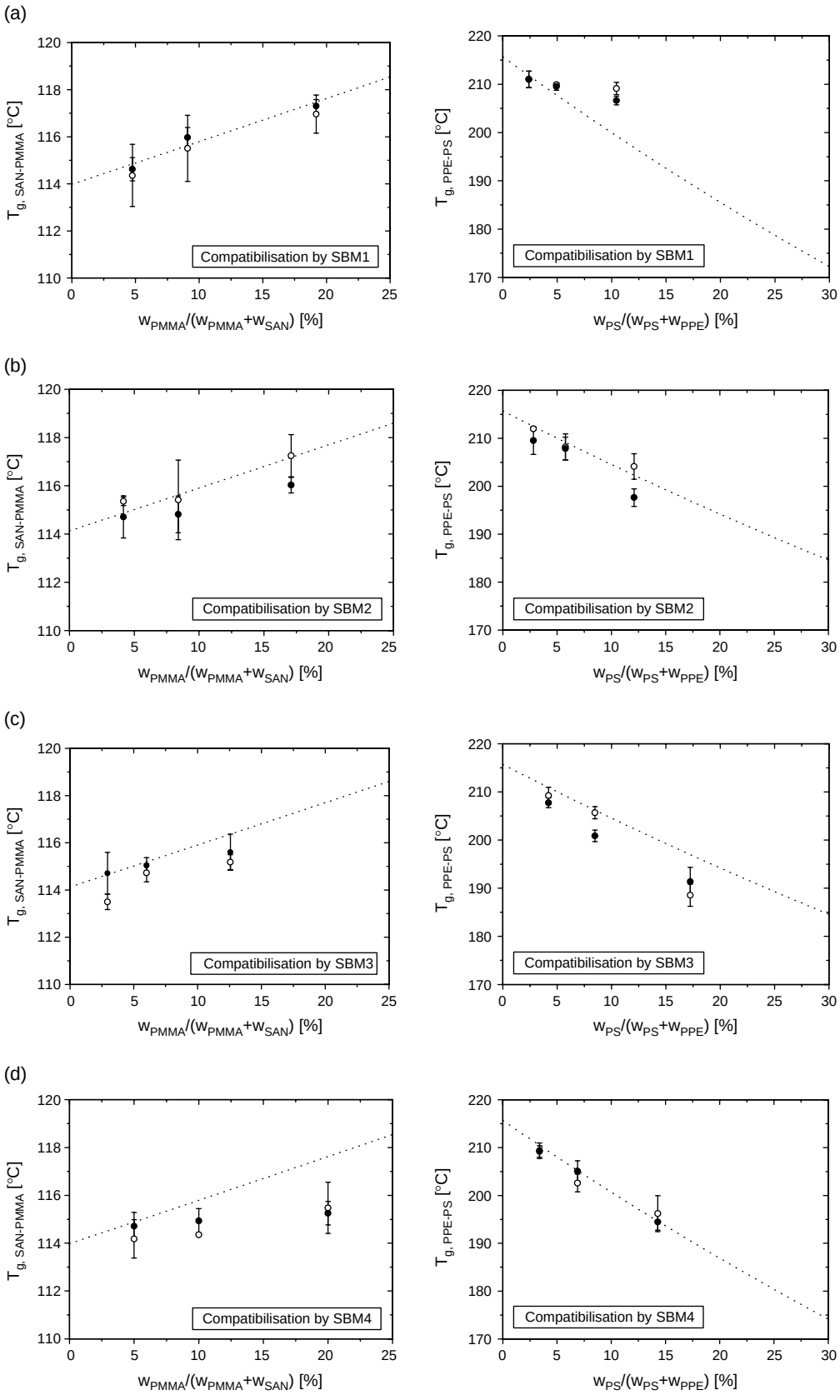

Fig. 10. Glass transitions of compatibilised blends following extrusion and injection-moulding, values obtained by DSC. Left side: glass transitions of the SAN-rich phase. Right side: glass transitions of the PPE-rich phase. Open symbols show the glass transition temperature following extrusion, full symbols denote the glass transition temperature following injection-moulding. The dashed line shows the theoretical prediction of homogeneously mixed PPE/PS and SAN/PMMA phases, respectively (according to Couchman and Fox, respectively).

general, a further melt-processing step involving shear and elongational flows can lead to significant variations of both thermal properties as well as morphological features. For comparison, the results of the thermal analysis of all injection-moulded specimens are included in Fig. 10 (solid symbols).

In most instances, the glass transition temperatures of the various blends appear to be similar within experimental error, independent of the processing history. These experimental observations would indicate the formation and development of similar blend morphologies as a function of SBM type and content as for the extruded samples. Nevertheless, small deviations in the glass transition behaviour of the injection-moulded blends as compared to the extruded blends can be observed, especially at high SBM contents. A slightly decreased glass transition temperature of the PPE containing 20 wt% of SBM1 indicates either starting micelle formation in the PPE phase or a transfer of SBM1 to the interface. Similar results are obtained for 20 wt% of SBM2, where the glass transition temperatures of both SAN and PPE are decreased. This observation, again, supports the assumption that SBM2 is partially removed from the interface and appears as micelles in the PPE phase. Finally, the second melt-processing step of the PPE/SAN blend containing SBM3 has led to an increased glass transition temperature of the SAN and a decreased T_g of the PPE, both effects relating to an improved segmental mixing PS with PPE and PMMA with SAN, respectively. Therefore, an enrichment of SBM3 at the interface can be assumed.

3.5. Morphology of blends following injection-moulding

In order to verify the predictions of the final blend morphologies based on the above presented thermal properties, a detailed TEM characterisation of the injection-moulded samples was carried out. Specimens were prepared from the core of the injection-moulded specimens in order to avoid the additional influence of the fast cooling rates of the blends experienced near the mould surfaces. Although a correlation of the final mechanical properties of such blends would require a detailed evaluation of the morphology in the skin and core region of injection-moulded specimens, the aim of this part to verify the influence of a second melt-processing step on the morphological development justifies the analysis of the core region.

The uncompatibilised PPE/SAN blend revealed a significant coarsening following reprocessing, as shown in Fig. 11(a) and (b). Here, two TEM micrographs at different magnifications are presented in order to fully highlight this structure. This increase of the average phase size is attributed to shear-induced coalescence and Ostwald ripening inside the plasticising unit. As a result of the high injection-rate, combined with the relatively low melt temperature, the break-up process of the PPE (dark) phase is suppressed and the specimens show some anisotropy [41]. Nevertheless, SAN still forms the more continuous phase, i.e. the matrix, and the continuity of PPE is slightly increased with respect to the extruded blend, see Fig. 5(a) for comparison.

As discussed in the context of the DSC experiments, most distinct differences in blend morphology are expected for the highest weight fractions of SBM. Representative TEM micrographs of the compatibilised blends containing 20 wt% of the various SBM types are shown in Fig. 11(c)–(f). These images clearly highlight the good agreement between the predictions based on the thermal features of the blends and the actual morphologies. With regard to SBM1, micelles of SBM are still found in the SAN phase; however, they also start to form in the PPE phase. As a result of this complex microstructure—SBM1 at the interface and as micelles in both phases—a reliable and exact determination of the SBM distribution is not trivial. As most of the SBM is found either as micelles in the SAN or at the interphase, these two processes are dominant for the development of the morphology, similar to the behaviour observed after extrusion.

With regard to SBM2, the interfacial situation and, subsequently, the distribution of SBM is modified after injection-moulding as compared to the previous extrusion step. Although the ‘raspberry morphology’ is mostly maintained at the interface, micelles and skin–core particles are formed in the PPE phase. This behaviour is a result of several influencing factors. Firstly, the morphology coarsens during the subsequent processing step. As a result, the specific surface of the PPE phase is reduced and, therefore, the saturation point for the compatibiliser is reached at lower SBM contents. The remaining compatibiliser induces micellation either in the SAN or in the PPE; however, the molecular composition of this particular SBM prefers the PPE phase as the enthalpic interaction between PPE and PS is significantly higher than that between SAN and PMMA. In addition, cross-linking of the polybutadiene can occur steadily at elevated temperatures, an effect that should not be neglected. Even the addition of stabilisers prevents this degradation only partially [35]. As a result, the SBM phase immobilises and, thus, the ability to reach thermodynamic equilibrium is reduced.

A further interesting detail seen in the TEM micrograph in Fig. 11(d) allows the evaluation of the structure of the SBM2 micelles: (1) the micelles in the PPE phase appear to contain PMMA, indicated by a small white core, and (2) the absence of SB diblock micelles highlights that the degradation of the PMMA block is low and that the thermal stability of this particular SBM is sufficient for injection-moulding at elevated temperatures.

In the case of SBM3, a co-continuous morphology is developed (Fig. 11(e)), the two phases are formed by SAN and PPE including SBM micelles, respectively. As discussed before, the tendency of SBM3 to form micelles in the PPE phase is a result of the longer PS block. In contrast to the morphology obtained following extrusion, here, additional core–shell particles are present in the PPE phase and, qualitatively, more SBM is located at the interface. Again, these factors not only reduce the viscosity of the PPE, but also increase the volume content of the PPE phase, thereby making a continuous PPE phase more favourable.

The situation following injection-moulding of the blend compatibilised with SBM4 is comparable to that with SBM2,

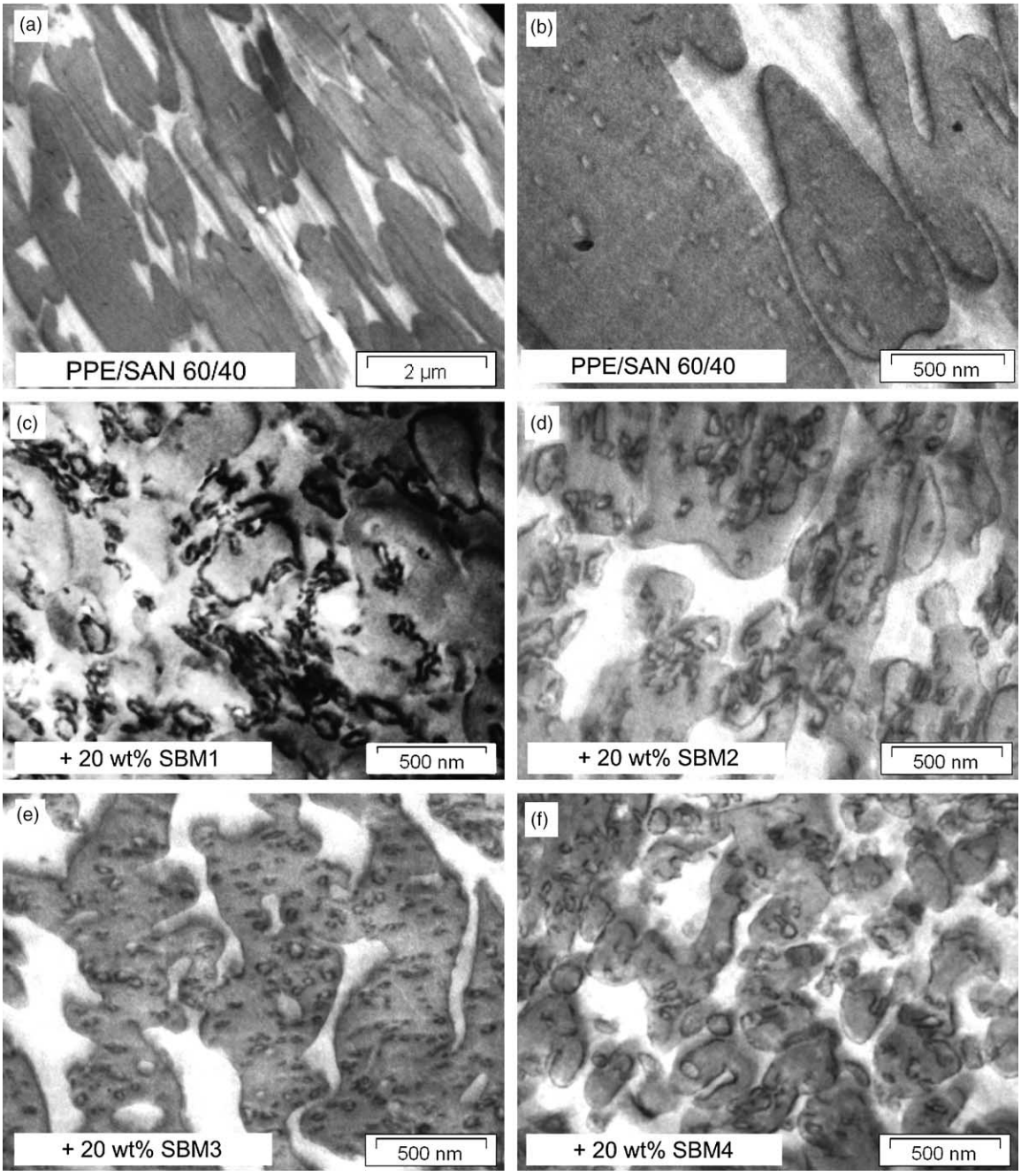

Fig. 11. TEM micrographs of melt-processed PPE/SAN blends following injection-moulding, uncompatibilised and after compatibilisation by 20 wt% SBM—effect of different SBM materials on compatibilisation (SBM1 = $S_{28}B_{36}M_{36}^{105}$, SBM2 = $S_{33}B_{34}M_{33}^{94}$, SBM3 = $S_{50}B_{27}M_{23}^{126}$, SBM4 = $S_{40}B_{20}M_{40}^{90}$; SAN bright, PPE dark, PB midblock of SBM black).

as most of the compatibiliser remains located at the interface and some micelles are formed in the PPE phase. However, the phase size is significantly larger in the latter case, reflecting the increased mobility of SBM with a decreasing PB content. As a consequence, the efficiency of dispersion is improved.

Comparing the blend morphologies shown in Figs. 5, 7 and 11, it becomes obvious that the continuity of the PPE phase is increased by the secondary injection-moulding process. This effect can be mostly attributed to the micellation of the SBM in the PPE phase. The tendency of SBM to form micelles in PPE is increased by an increasing ratio of the block lengths of PS to PMMA. Furthermore, the length of the middle block influences the dispersion efficiency and, subsequently, the overall blend morphology. The micelle formation is comparable between the SBM grades with balanced end block ratios. Independent of processing history, the SBM block copolymers lead to a reduced coalescence of the respective blend partners, an effect which is clearly demonstrated by comparing the phase size of the uncompatibilised and the compatibilised blends. Finally, the final blend morphologies are quite complex, as both the

microstructure (continuity of PPE and SAN, core–shell particles) as well as the nanostructure (micelle formation, raspberry morphology) are both influenced by the SBM type and content as well as the particular shear and elongational flows.

3.6. Dynamic mechanical properties of injection-moulded blends as a function of temperature

Dynamic mechanical analysis is often employed to determine the performance of polymer blends under temperature loads. In particular, the stiffness of the blends in the linear-elastic regime can be evaluated with increasing temperature as a function of SBM type and content. Such experiments also provide further information regarding the blend morphology as well as the molecular arrangement of the components. The dynamic mechanical properties of a compatibilised multiphase blend mainly depend on the properties of the components, the composition, the morphology and other effects of the compatibilisation such as the dispersion and distribution of the compatibiliser.

3.6.1. Theoretical consideration of DMTA properties of compatibilised blends

Scobbo [42] identified two main constraints imposed on the motion of molecular segments in the vicinity of the interface: (a) the presence of rigid phases and (b) the presence of chemical and physical bonds between the two phases, which in a general sense includes the presence of interfacial agents such as block copolymers. As the change in free volume and, thus, the molecular mobility of both components is low below the glass transition of both phases, the storage modulus, E', and the loss modulus, E'', of PPE and SAN, and of the blend are relatively constant. If the temperature is increased to a value above the SAN glass transition but below the PPE glass transition, the change of free volume of the SAN becomes distinct.

In general, three factors are influencing the behaviour of E' in this temperature range: (1) The overall morphology of the blend, i.e. the continuity of both phases. If PPE forms the matrix, the change of free volume is less pronounced and the modulus remains at a higher level, whereas SAN as a matrix will show a more pronounced softening [1]. (2) The degree of dispersion. An improved dispersion leads to a finer morphology and, thus, to an increased interfacial area of the blend. In turn, the storage modulus of blends with a finer morphology has been shown to depend more strongly on the temperature [1,10,42]. As compatibilisers such as block copolymers reduce the phase size, a reduction of the storage modulus at these elevated temperatures is observed. (3) The molecular composition of the compatibilising block copolymer. The mechanical coupling between the two phases is generally improved by higher molecular weight copolymers, as the interfacial width and the adhesion between the immiscible polymers is increased [40]. In addition, the mechanical coupling between the two phases appears to also influence E'' in this temperature range. Independent of the polymer blend partners, Scobbo observed decreasing E'' values after the addition of suitable compatibilisers, indicating a reduction of the viscous energy dissipation. This effect is attributed to the reduced internal friction between the two phases as the block copolymer improves the coupling and, thus, restricts molecular motion [42].

When increasing the temperature to a value above the glass transition of both blend partners, the loss modulus E'' especially is affected by the compatibilisation [42]. As the compatibilised blend is linked across the interface by the block copolymers, the molecular motion of the blend, i.e. the relaxation of the respective phases, is restricted. Due to this reduced motion, the maximum of the loss modulus at the higher temperature glass transition is reduced. As similar results are observed by decreasing the relative amount of the high T_g-phase and by refinement of the morphology [10], the improved compatibilisation efficiency steadily promotes a less pronounced maximum of the loss modulus.

3.6.2. Experimentally observed properties following injection-moulding

In order to compare these theoretical considerations with the experimental results, the thermo-mechanical properties of the PPE/SAN blend before and after compatibilisation with increasing weight fraction of SBM1 are shown in Fig. 12. As can be seen, two distinct glass transitions appear for the uncompatibilised blend, related to the PPE and the SAN phase. The morphology with SAN as the continuous phase is reflected by the behaviour of the storage modulus, showing a pronounced drop as the temperature exceeds the glass transition of SAN. In the temperature region above the glass transition of SAN and below the glass transition of PPE, SAN is in the rubbery state and the still glassy PPE restricts the molecular motion. The relatively high level of the storage modulus indicates a certain continuity of the PPE phase but no co-continuity, in agreement with the TEM observations. The presence of two continuous phases would be indicated by an even higher modulus and a more stable plateau region, in

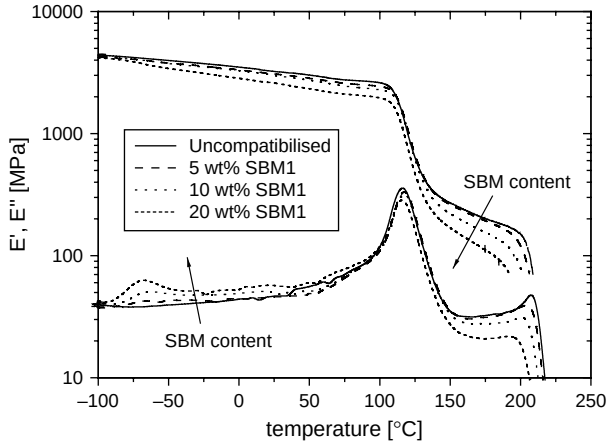

Fig. 12. Dynamic mechanical thermal properties PPE/SAN blends following injection-moulding—uncompatibilised blend and effect of compatibilisation by various amounts of SBM1 ($S_{28}B_{36}M_{36}^{105}$) on storage and loss modulus.

contrast to the steadily decreasing storage modulus observed in the experiment for temperatures above the glass transition of the SAN.

With the addition of SBM1, one additional low temperature glass transition is observed, representing the PB of the triblock terpolymer. The intensity of the corresponding E'' peak scales with the amount of compatibiliser. The shape of the glass transition of SAN is not altered. Nevertheless, the temperature-dependence of the storage modulus in the temperature range between the T_g of SAN and PPE becomes more pronounced. This decreasing modulus with increasing SBM content reflects the compatibilisation of the system and, more precisely, the resulting decreased phase size. Additionally, the shift of both the onset to the storage modulus drop as well as of the maximum of the loss modulus are evidence for a decreasing glass transition of PPE with increasing SBM content, as the PS interpenetrates into the PPE phase. The peak intensity of E'' at the T_g of PPE continuously decreases, in reasonable agreement with the observations stated by Scobbo [42]. Finally, the decreasing intensity of the loss modulus in the temperature region between the glass transitions of SAN and PPE should be noted, which is assumed to relate to the reduced molecular motion as the compatibiliser is located at the interface. A similar behaviour is observed for the blends compatibilised with increasing content of SBM2.

The effect of compatibilisation on the thermo-mechanical behaviour of the PPE/SAN blend by the addition of increasing weight fractions of SBM3 is shown in Fig. 13. Here, significant differences to the previously discussed observations are found. In contrast to SBM1 and SBM2, the storage modulus of these blends maintains the level of the uncompatibilised blend in the temperature region between the glass transitions of SAN and PPE, independent of SBM content. This enhanced stiffness can be attributed to the improved continuity of the PPE phase approaching a co-continuous morphology. Furthermore, the loss modulus remains nearly constant. The maximum of E'', the glass transition temperature of PPE, is significantly larger in these cases as those of blends compatibilised with SBM1 and SBM2. Based on the TEM observations, this effect is related to the distribution of the SBM3 which is located mainly in the PPE phase and not at the interface. In order to further highlight the differences between SBM2 and SBM3, the thermo-mechanical behaviour of these respective blends compatibilised with 20 wt% of SBM is summarised in Fig. 14.

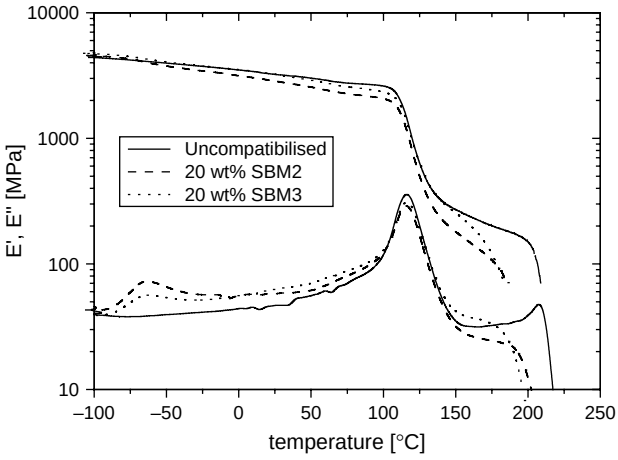

Fig. 14. Dynamic mechanical thermal properties of PPE/SAN blends following injection-moulding—comparison between the uncompatibilised blend and compatibilisation by SBM2 and SBM3, respectively.

Finally, the thermo-mechanical behaviour of blends compatibilised with SBM4 is similar to that observed for blends containing SBM1 and SBM2, i.e. the desired compatibilisation effect is demonstrated (Fig. 15). However, two distinctions become apparent: First, as a result of the lower content in the triblock terpolymer, the glass transition of the PB phase is less pronounced. Secondly, the effect related to the interfacial activity—higher temperature-dependence of the storage modulus and decreased loss modulus above the glass transition of SAN—is more distinct. The shorter PB block leads to a higher mobility and, in turn, a higher interfacial activity (Fig. 15).

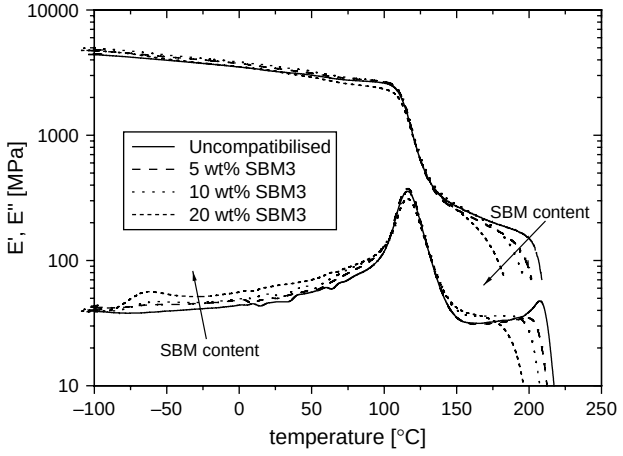

Fig. 13. Dynamic mechanical thermal properties of PPE/SAN blends following injection-moulding—uncompatibilised blend and effect of compatibilisation by various amounts of SBM3 ($S_{50}B_{27}M_{23}^{126}$) on storage and loss modulus.

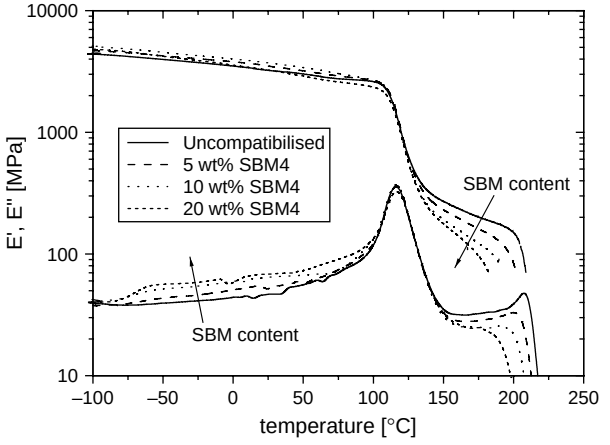

Fig. 15. Dynamic mechanical thermal properties of PPE/SAN blends following injection-moulding—uncompatibilised blend and effect of compatibilisation by various amounts of SBM4 ($S_{40}B_{20}M_{40}^{90}$) on storage and loss modulus.

In summary, there exists a correlation between theoretical predictions of the thermo-mechanical properties and the actual results for all compatibilised blends, irrespective of SBM type and content. The experimentally obtained blend properties, therefore, reflect the differences in the morphological features as observed by the detailed transmission electron microscopic investigations.

4. Conclusions

Immiscible PPE/SAN blends of potential commercial interest were compatibilised by systematically varied SBM triblock terpolymers in order to ensure compatibilisation and to improve the otherwise poor mechanical properties. However, the application of economically favoured melt-processing techniques of such compatibilised PPE/SAN blends leads to significantly different morphologies as observed for solvent-mediated systems since the number of influencing factors is strongly increased. These parameters include the significantly reduced residence time available to attain thermodynamic equilibrium, the presence of both high shear and temperature as well as the stronger influence of melt-rheological properties.

The systematic variation of the SBM block lengths carried out in this study leads to the following general conclusions: Symmetric SBM types with equal block lengths, such as SBM2 ($S_{33}B_{34}M_{33}^{94}$), act as a compatibiliser as they locate at the interface and form the desired raspberry morphology. Similar results are observed for nearly symmetric SBM types, such as SBM1 (slightly reduced block lengths of PS while the ratio between PMMA and PB remains constant, $S_{28}B_{36}M_{36}^{105}$), and for SBM types with symmetric end blocks such as SBM4 (equal length of the end blocks while the PB content is reduced, $S_{40}B_{20}M_{40}^{90}$).

In contrast, the addition of SBM types with a PS block length which is significantly higher than the block length of PMMA, such as SBM2 ($S_{50}B_{27}M_{23}^{126}$), leads to a strong micelle formation in the PPE and the interfacial activity remains low. The observation most likely is due to the strength of the interactions between the end blocks of SBM and the respective blend components. Balanced lengths of PS and PMMA lead to a well-defined swelling behaviour in each blend phase and, thus, localisation of SBM at the interface is ensured. In contrast, a significantly higher swelling power of the PS in PPE compared to PMMA in SAN is observed for longer PS block lengths and, thus, localisation in the PPE phase is favoured in this case. Nevertheless, the dispersion efficiency of all triblock terpolymers is lower than those of diblocks [5] as a result of the presence of the PB middle block. SBM triblock terpolymers can be used as effective interfacial agents for the compatibilisation of PPE/SAN blends as long as the end blocks of the SBM have nearly similar length.

The morphology of the pure SBM is strongly controlled by the respective block lengths of the triblock terpolymer, and these morphological features can be correlated with the efficiency of compatibilisation. In the present blend system, SBM1 as well as SBM2 form completely lamellar morphologies (ll); in contrast, SBM3 is located at a transition region between lamellar morphologies (ll) and cylindrical morphologies (lc, uc–lc). Cc morphologies are characterised by a PS matrix with embedded cylinders of PMMA which are covered by PB; and, finally, SBM4 shows lamellae of PS and PMMA with PB cylinders at the interface (lc). The lamellar structures of PS and PMMA (SBM1, SBM2, SBM4) reflect the nearly equal lengths of the end blocks and are, therefore, suitable to compatibilise the blend in an efficient way.

The thermal properties of all blend systems as obtained by differential scanning calorimetry investigations are in good agreement with the morphologies observed after extrusion and injection-moulding. Interestingly, the structures remained relatively stable during the second melt-processing step, except for the discussed micelle formation, indicating that no significant change of the segmental mixing of the SBM with the blend components has occurred.

In addition, the dynamic mechanical thermal analysis further supports the interpretation of the blend morphologies. Both the storage as well as the loss modulus in the temperature range between the glass transition temperatures of SAN and PPE can be used as a sensitive indicator for the compatibilisation efficiency. Blends successfully compatibilised with SBM1, SBM2, and SBM4 show an increased dependence of the storage modulus on the temperature as well as a decrease in loss modulus; in contrast, blends compatibilised by SBM3 show a different behaviour reflecting the reduced dispersion efficiency and the tendency to form micelles in the PPE.

The systematic correlation of SBM structure and blend morphology presented in this study has allowed the identification of suitable compatibilisation agents for immiscible PPE/SAN blends. The resulting increases in blend toughness and minimised losses in stiffness will be presented in a following paper.

Acknowledgements

This work has been supported by the Deutsche Forschungsgemeinschaft within SFB 481 (project A10). We are grateful to Dr. M. Weber (BASF AG, Ludwigshafen) and to MEP Europe, Düsseldorf for providing the SAN and PPE, respectively. We gratefully acknowledge helpful discussions with K. Hamada and Y. Morishita. Furthermore, the authors are indebted to D. Danz (Macromolecular Chemistry II, University of Bayreuth) for synthesising some of the SBM triblock terpolymers, and to C. Kunert (Polymer Engineering, University of Bayreuth and SFB 481, Z2, respectively) for the TEM investigations.

References

[1] Paul DR, Bucknall CB. 2nd ed. Polymer blends, vols. 1 and 2. Wiley: New York; 2000.
[2] Utracki LA. Commercial polymer blends. 1st ed. London: Chapman and Hall; 1998 [chapters 6–9].
[3] Kressler J, Kammer HW. Acta Polym 1987;38(11):600–2.
[4] Merfeld GD, Karim A, Majumdar B, Satija SK, Paul DR. J Polym Sci, Part B:Polym Phys 1998;36(17):3115–25.

[5] Auschra C, Stadler R. Macromolecules 1993;26(24):6364–77.
[6] Lach R, Grellmann W, Weidisch R, Altstadt V, Kirschnick T, Ott H, et al. J Appl Polym Sci 2000;78(11):2037–45.
[7] Kirschnick T, Gottschalk A, Ott H, Abetz V, Puskas J, Aldstadt V. Polymer 2004;45(16):5653–60.
[8] Gottschalk A, Muhlbach K, Seitz F, Stadler R, Auschra C. Macromol Symposia 1994;83:127–46.
[9] Fekete E, Foldes E, Damsits F, Pukanszky B. Polym Bull 2000;44(4): 363–70.
[10] Quintens D, Groeninckx G. Polym Eng Sci 1991;31(16):1207–14.
[11] Lee CH, Lee SG, Kang SW, Yun S, Kim JH, Choe S. Polymer-Korea 1999;23(1):98–104.
[12] Creton C, Kramer EJ, Hui CY, Brown HR. Macromolecules 1992;25(12): 3075–88.
[13] Creton C, Kramer EJ, Hadziioannou G. Macromolecules 1991;24(8): 1846–53.
[14] Anastasiadis SH, Gancarz I, Koberstein JT. Macromolecules 1989;22(3): 1449–53.
[15] Sundararaj U, Macosko CW. Macromolecules 1995;28(8):2647–57.
[16] Milner ST, Xi HW. J Rheol 1996;40(4):663–87.
[17] Gottschalk A, Seitz F, Stadler R, Auschra C. DE 42 40 455 A1 (1992) BASF AG, Germany.
[18] Fowler ME, Barlow JW, Paul DR. Polymer 1987;28(12):2145–50.
[19] Suess M, Kressler J, Kammer HW. Polymer 1987;28(6):957–60.
[20] Kressler J, Kammer HW. Acta Polym 1987;38(11):600–2.
[21] Stadler R, Auschra C, Beckmann J, Krappe U, Voigt-Martin I, Leibler L. Macromolecules 1995;28(9):3080–97.
[22] Kitayama T, Shinozaki T, Masuda E, Yamamoto M, Hatada K. Polym Bull 1988;20(6):505–10.
[23] Ballard DGH, Bowles RJ, Haddleton DM, Richards SN, Sellens R, Twose DL. Macromolecules 1992;25(22):5907–13.
[24] Schlaad H, Schmitt B, Müller AHE. Angew Chem—Int Ed 1998;37(10): 1389–91.
[25] Hamada K, Ishiura K, Kato M, Yaginuma S. JP 99-236,445 (1999), EP 1,078,942 A1 (2001) Kuraray Co. Ltd, Japan.
[26] Wool RP. Polymer interfaces. 1st ed. Munich: Carl Hanser; 1995 [chapter 7].
[27] Trent JS, Scheinbeim JI, Couchman PR. Macromolecules 1983;16(4): 589–98.
[28] Bates FS, Fredrickson GH. Annu Rev Phys Chem 1990;41:525–57.
[29] Abetz V, Goldacker T. Macromol Rapid Commun 2000;21(1):16–34.
[30] Wu S. Polym Eng Sci 1987;27(5):335–43.
[31] Pahl MH. Praktische Rheologie der Kunststoffschmelzen und Lösungen. 1st ed. Düsseldorf: VDI-Verlag; 1983.
[32] Jordhamo GM, Manson JA, Sperling LH. Polym Eng Sci 1986;26(8): 517–24.
[33] Chen TH, Su AC. Polymer 1993;34(23):4826–31.
[34] Utracki LA. J Rheol 1991;35(8):1615–37.
[35] Auschra C, Stadler R. Polym Bull 1993;30(3):305–11.
[36] Everaert V, Aerts L, Groeninckx G. Polymer 1999;40(24):6627–44.
[37] Everaert V, Groeninckx G, Pionteck J, Favis BD, Aerts L, Moldenaers P, et al. Polymer 2000;41(3):1011–25.
[38] Kim JR, Hudson SD, Jamieson AM, Manas-Zloczower I, Ishida H. Polymer 2001;42(9):4281–8.
[39] Couchman PR. Macromolecules 1978;11(6):1156–61.
[40] Auschra C, Stadler R, Voigt-Martin IG. Polymer 1993;34(10):2094–110.
[41] Paul DR, Bucknall CB. Polymer blends. 2nd ed. New York: Wiley; 2000 [chapter 16].
[42] Scobbo JJ. Polym Test 1991;10(4):279–90.